# Supplemental Material for "Shortcuts to Thermodynamic quasistaticity"

Artur Soriani,[1,*] Eduardo Miranda,[1] Sebastian Deffner,[2] and Marcus V. S. Bonança[1]

[1]*Gleb Wataghin Institute of Physics, University of Campinas, Campinas, São Paulo 13083–950, Brazil*
[2]*Department of Physics, University of Maryland, Baltimore County, Baltimore, Maryland 21250, USA*

(Dated: October 19, 2022)

In these Supplementary Materials we provide (i) an overview of adiabatic perturbation theory, (ii) further technical details for the driven Ising chain, and (iii) a comparison of our new method with invariant based reverse engineering for the parametric harmonic oscillator.

*Adiabatic perturbation theory* (APT) [1] is a perturbative generalization of the adiabatic theorem. An exact solution of the Schrödinger equation can be written as

$$|\psi_n(t)\rangle = e^{i\phi_n(t)} \sum_{p=0}^{\infty} \sum_m C_{mn}^{(p)}(t)\, |m(\lambda)\rangle\,, \tag{1}$$

where $\phi_n(t)$ is the adiabatic phase and the coefficients $C_{mn}^{(p)}(t)$ represent the $p$th order corrections to the adiabatic solution, which is Eq. (3) of the main text. For $p = 0$, we simply have $C_{mn}^{(0)}(t) = \delta_{mn}$, and Eq. (1) truncated at this order reproduces the adiabatic approximation.

For $p > 0$, the coefficients $C_{mn}^{(p)}(t)$ can be systematically calculated [1]. For instance, for $p = 1$ and $m \neq n$ we have

$$C_{mn}^{(1)}(t) = i\hbar \left( \frac{M_{mn}(\lambda)}{E_{mn}(\lambda)} - e^{i\phi_{mn}(t)} \frac{M_{mn,i}}{E_{mn,i}} \right), \tag{2}$$

where

$$M_{mn}(t) = \dot{\lambda}(t) \frac{F_{mn}(\lambda)}{E_{mn}(\lambda)}, \tag{3}$$

$F_{mn}$ are the matrix elements of the generalized force [Eq. (1) of the main text] and we introduced $E_{mn}(\lambda) \equiv E_m(\lambda) - E_n(\lambda)$ and $\phi_{mn}(t) \equiv \phi_m(t) - \phi_n(t)$.

For the purposes discussed here, higher order coefficients can be obtained from the first order coefficient with iterative substitutions. For example, $C_{mn}^{(2)}$ with $m \neq n$ is given by Eq. (2) with the change $M_{mn}(t) \to i\hbar \frac{d}{dt} \frac{M_{mn}(t)}{E_{mn}(\lambda)}$. We can gauge how accurate the theory is by using the so-called quantitative adiabatic condition [2, 3]

$$\hbar \frac{M_{mn}(t)}{E_{mn}(\lambda)} \ll 1, \tag{4}$$

which can be evaluated at any point in time $t$ of a given process.

*Transverse field Ising chain* The Hamiltonian of the system is given in Eq. (8) of the main text. We assume an even number of spins and periodic boundary conditions, while taking $\hbar = 1$. After a Jordan-Wigner transform, a Fourier transform and a Boguliobov transform [4], this Hamiltonian is brought to diagonal form, represented by non-interacting fermions with dispersion

$$\epsilon_k(\Gamma) = \sqrt{(\Gamma - J\cos k)^2 + J^2 \sin^2 k}, \tag{5}$$

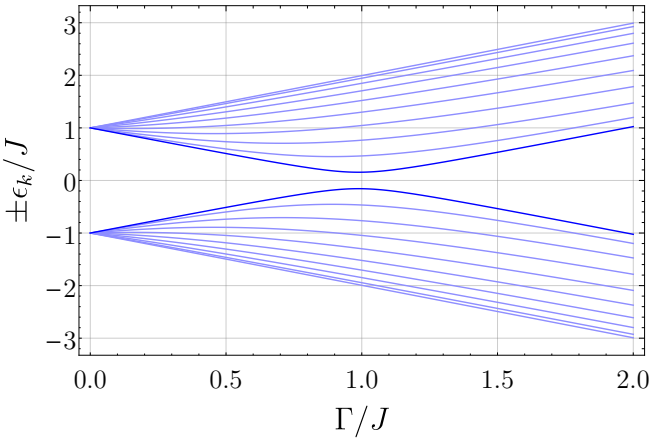


FIG. 1. Eigen-energies of the transverse field Ising chain [Eq. (5)] versus the external field $\Gamma$, for $N = 20$ and all possible values of $k$.

for $N$ allowed values of momentum

$$k_n = (2n+1)\frac{\pi}{N}, \tag{6}$$

given integer $n$ between $-N/2$ and $N/2 - 1$. Figure 1 shows the energies of Eq. (5) as a function of $\Gamma$ for $N = 20$, where the energy gap between the two lowest energy levels is seen to shrink at $\Gamma = J$, the quantum critical point (QCP) of the system.

If the system starts the process in its initial ground state, its dynamics can be simplified into the dynamics of $N/2$ two-level systems (known as Landau-Zener systems), one for each positive value of $k$ [5]. The evolved ground state can be written as

$$|\psi(t)\rangle = \bigotimes_{k>0} \Big( u_k(t)\, |{\downarrow_k}\rangle - v_k(t)\, |{\uparrow_k}\rangle \Big), \tag{7}$$

where $|{\uparrow_k}\rangle$ and $|{\downarrow_k}\rangle$ form a basis of the two-level system labeled by $k$. Placing Eq. (7) into Schrödinger's equation leads to (omitting the time-dependences of $u_k$, $v_k$ and $\Gamma$)

$$\begin{aligned} i\,\dot{u}_k &= -(\Gamma - J\cos k)\, u_k - J\sin k\, v_k, \\ i\,\dot{v}_k &= -J\sin k\, u_k + (\Gamma - J\cos k)\, v_k. \end{aligned} \tag{8}$$

The numerical results of presented here and in the main text were obtained from the standard fourth-order Runge–Kutta method applied to Eq. (8). The magnetization per spin can be expressed as

$$\mu(t) = \frac{1}{N} \sum_{k>0} \Big( |u_k|^2 - |v_k|^2 \Big)\,. \tag{9}$$

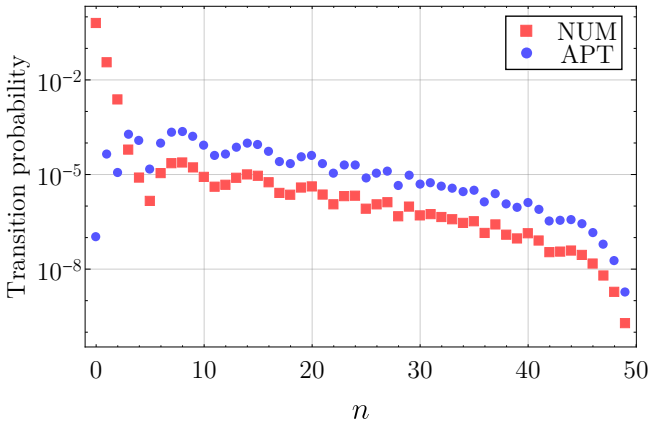


FIG. 2. Transition probabilities between the ground state and an excited state with a single pair of fermions with momenta $k_n$ [Eq. (6)], as a function of $n$, in a process that crosses the QCP of the TI chain with $N = 100$ and $J\tau = 50$. The red squares represent the result from numerical integration of Eq. (8), while the blue circles represent the analytical result from first-order APT.

where $u_k$ and $v_k$ are calculated from Eq. (8).

Figure 2 shows the transition probabilities in a process starting in the ground state of the paramagnetic phase and ending in the ferromagnetic phase of the TI chain, the same QCP-crossing process considered in the main text. In it, we display only transitions to states reached by the creation of a single pair of fermions with momenta $k_n$ [given in Eq. (6)], which means that the relevant energy gap increases as $n$ (the variable in the horizontal axis) increases. There is a clear downward trend, which confirms the notion that transition probabilities are higher for pairs of neighbouring energy levels. For small $n$, the probabilities decrease exponentially with $n$, which means that only the lowest energy eigenstates contribute meaningfully to the dynamics, while the rest of the eigenstates can be ignored in the determination of protocols such as FQA.

In any process, the linear protocol (LIN) is

$$\Gamma_{\rm LIN}(t) = \Gamma_i + (\Gamma_f - \Gamma_i)\,\frac{t-t_i}{\tau}. \tag{10}$$

The FQA protocol [6] is obtained by solving Eq. (6) of the main text for the two lowest energy states,

$$\Gamma_{\rm FQA}(t) = J\cos k_0 + J\sin k_0 \frac{\alpha(t)}{\sqrt{1-\alpha^2(t)}}, \tag{11}$$

where $k_0 = \pi/N$,

$$\alpha(t) = \cos\theta_{k_0,i} + (\cos\theta_{k_0,f} - \cos\theta_{k_0,i})\,\frac{t-t_i}{\tau} \tag{12}$$

and

$$\theta_k(\Gamma) = \arctan\left(\frac{J\sin k}{\Gamma - J\cos k}\right). \tag{13}$$

Equation (7) of the main text cannot be solved analytically in this case, so we solved it numerically to obtain FQ2.

The UQA [7] and UQ2 protocols are obtained, respectively, by solving Eqs. (6) and (7) of the main text with the substitution $F_{mn}(\lambda) \to \partial_\lambda E_{mn}(\lambda)$. For $\Gamma_f < \Gamma_i$, their explicit forms are

$$\Gamma_{\rm UQA}(t) = J\begin{cases} \cos k_0 + \sin k_0 \sqrt{\left(\sin\theta_{k_0,i} + (1-\sin\theta_{k_0,i})\,\dfrac{t-t_i}{t_1-t_i}\right)^{-1} - 1}, & t < t_1; \\ \cos k_0 - \sin k_0 \sqrt{\left(\sin\theta_{k_0,f} + (1-\sin\theta_{k_0,f})\,\dfrac{t_f-t}{t_f-t_1}\right)^{-1} - 1}, & t > t_1; \end{cases} \tag{14}$$

and

$$\Gamma_{\rm UQ2}(t) = J\begin{cases} \cos k_0 + \sin k_0 \sqrt{\csc^2\theta_{k_0,i}\exp\left(\sqrt{2}\,\mathrm{erf}^{-1}\left[\frac{t-t_i}{t_2-t_i}\mathrm{erf}\left(\sqrt{\log\sin\theta_{k_0,i}}\right)\right]\right)^2 - 1}, & t < t_2; \\ \cos k_0 - \sin k_0 \sqrt{\csc^2\theta_{k_0,f}\exp\left(\sqrt{2}\,\mathrm{erf}^{-1}\left[\frac{\epsilon_{k_0,f}}{\epsilon_{k_0,i}}\frac{t_f-t}{t_f-t_2}\mathrm{erf}\left(\sqrt{\log\sin\theta_{k_0,i}}\right)\right]\right)^2 - 1}, & t > t_2; \end{cases} \tag{15}$$

In Eq. (15), $\mathrm{erf}(z) = \frac{2}{\sqrt{\pi}}\int_0^z e^{-x^2}dx$ is the error function and $\mathrm{erf}^{-1}$ is its inverse. The times when UQA and UQ2 cross the QCP are $t_1$ and $t_2$ respectively, and they are given by weighted arithmetic mean values of $t_i$ and $t_f$. For UQA, the weights are $1/(1-\sin\theta_{k_0})$, while for UQ2, they are $\epsilon_{k_0}/\mathrm{erf}\left(\sqrt{\log\sin\theta_{k_0}}\right)$.

Figure 3 shows the state diagrams of the reverse processes starting in the ground state. In the entirely paramagnetic process of Fig. 3a, we can see that FQA outperforms FQ2, because it naturally has a small time derivative at $t_i$. Accordingly, it has a small first-order APT correction to the magnetization while still doing better than FQ2 at assuring APT, which makes it follow the EOS closely. This shows that FQA and FQ2 are complementary strategies: if the initial derivative of FQA is small, use it; otherwise, use FQ2. Conversely, Fig. 3b shows that FQA-like strategies will always have large $\dot{\lambda}_i$ when crossing a critical point, which makes FQ2-like strategies desirable for closely following

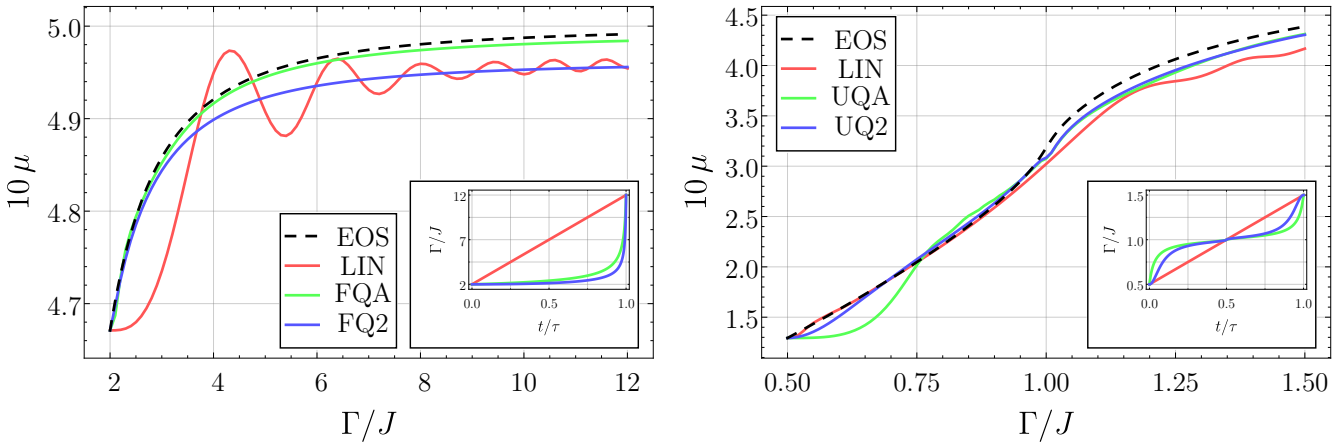


(a) (b)

FIG. 3. State diagrams of the time-reversed versions of the processes considered in the main text for the TI chain initially prepared in its ground state with $N = 100$. The insets show the time-dependence of each protocol. (a) Reverse paramagnetic process for $J\tau = 3$. (b) Reverse QCP crossing process for $J\tau = 50$.

the EOS.

*Lewis-Riesenfeld invariants: the parametric harmonic oscillator* The harmonic oscillator (HO) Hamiltonian, with mass $m$ and varying frequency $\omega$, is

$$H_{\rm HO}(\omega) = \frac{p^2}{2m} + \frac{k(\omega)q^2}{2}, \qquad k(\omega) = m\omega^2. \quad (16)$$

The generalized force reads $F_{\rm HO} = \partial_k H_{\rm HO} = q^2/2$, defined without the minus sign for convenience. The (non-equilibrium) state variable $K$, conjugate to $k$, can be calculated exactly from

$$K(t) = \frac{Y^2(t) + \omega_i^2 X^2(t)}{2m\omega_i\omega(t)} \left\langle H_{\rm HO}(\omega(t))\right\rangle^{(0)}, \quad (17)$$

where $\left\langle H_{\rm HO}(\omega(t))\right\rangle^{(0)}$ is the average energy calculated in the adiabatic limit, while $X$ and $Y$ are solutions to the classical equation of motion, $\ddot{Z} + \omega^2 Z = 0$, with initial conditions $X_i = 0 = \dot{Y}_i$ and $\dot{X}_i = 1 = Y_i$ [8–10].

The energetic cost of a given process, quantified as extra work above the quasistatic work, is

$$W_{\rm ex}(t) = (Q^*(t) - 1)\left\langle H_{\rm HO}(\omega(t))\right\rangle^{(0)}, \quad (18)$$

where (omitting the time-dependences of $X$, $Y$ and $\omega$)

$$Q^*(t) = \frac{\dot{Y}^2 + \omega^2 Y^2 + \omega_i^2\left(\dot{X}^2 + \omega^2 X^2\right)}{2\omega_i\omega} \quad (19)$$

is an adiabatic measure of the harmonic oscillator: whenever $Q^*(t) = 1$, the system is in the same state as an adiabatic process at time $t$.

The invariant-based inverse engineering (IIE) approach exploits the fact that the system's Hamiltonian admits a Lewis-Riesenfield invariant [11] of the form

$$I(t) = \frac{\left(b(t)p - m\dot{b}(t)q\right)^2}{2m} + \frac{m\omega_0^2 q^2}{2b^2(t)}, \quad (20)$$

as long as $b(t)$ solves the Ermakov equation

$$\ddot{b}(t) + \omega^2(t)b(t) = \frac{\omega_0^2}{b^3(t)} \quad (21)$$

and $\omega_0$ is an arbitrary constant.

Thus, the eigenstates of $I(t)$ are solutions to Schrödinger's equation. One then sets $\omega_0 = \omega_i$ and chooses $b(t)$ such that the eigenstates of $I(t)$ and of $H_{\rm HO}(\omega)$ coincide at $t_i$ and $t_f$ (up to irrelevant phases) [12]. The corresponding protocol $\omega_{\rm IIE}(t)$ is obtained from Eq. (21), and it guarantees, for any process duration $\tau$, the same final state as an adiabatic process. There is freedom in choosing the exact form for $b(t)$ — we chose the simplest polynomial in $t/\tau$ that satisfies the required boundary conditions. Note that, while $b(t)$ is a strict function of $t/\tau$, $\omega_{\rm IIE}(t)$ obtained from Eq. (21) is not. We shall see later on that the IIE protocol has some unique properties on the state diagram, owning to its invariant-based design.

Solving Eq. (6) of the main text for the HO with the proper boundary conditions gives us the FQA protocol [6]

$$\omega_{\rm FQA}(t) = \left(\frac{1}{\omega_i} + \left(\frac{1}{\omega_f} - \frac{1}{\omega_i}\right)\frac{t - t_i}{\tau}\right)^{-1}. \quad (22)$$

On the other hand, solving Eq. (7) of the main text with $\dot{\omega}_i = 0$ gives us the FQ2 protocol

$$\omega_{\rm FQ2}(t) = \omega_i \exp\left\{\mathrm{erf}^{-1}\left[\frac{t - t_i}{\tau}\mathrm{erf}\left(\sqrt{\log\frac{\omega_f}{\omega_i}}\right)\right]\right\}^2. \quad (23)$$

Figure 4 shows forward and backward processes for the same $\tau$ and an initial canonical distribution of inverse temperature $\beta_i$. Note in the insets that the forms of IIE and FQA in the backward process are simply their time-reversed forms of the forward process, but this is not the case for FQ2, given its requirement to set $\dot{\omega}_i = 0$ while not

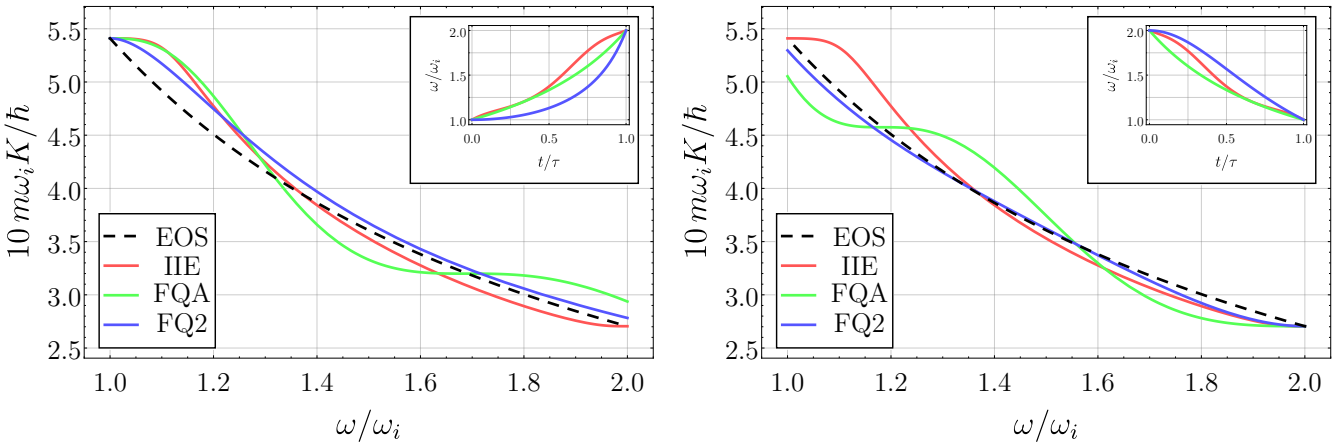


FIG. 4. State diagrams of the HO for an adiabatic (quasistatic) evolution (EOS), the IIE, the FQA and the FQ2 protocols for $\omega_i\tau = 3$ and $\beta_i\hbar\omega_i = 1$. The inset shows the form of the protocols. (a) forward process, starting in the top left corner; (b) backward process, starting in the the bottom right corner.

setting $\dot{\omega}_f$. We can clearly see that, out of the three protocols, FQ2 does the best job of keeping the evolution closer to the EOS at all times. Of course, FQA and FQ2 do not have the same exact final state predicted by the EOS, unlike IIE, which requires more information about the system and is, therefore, inaccessible in most cases. Peculiarly, IIE traces the exact same curve of the state diagram in the forward process (FIG. 4a) and in the backward process (FIG. 4b), which is a consequence of its invariant-based nature.

Figure 5 shows, at $t_f$, the excess state variable and excess work vs. $\tau$ in the forward process. We see, from Fig. 5a, that FQA achieves $K_{\rm ex} = 0$ for a specific small time in the range $1 < \omega_i\tau < 2$, while FQ2 gives an overall smaller $K_{\rm ex}$ for an arbitrary $\omega_i\tau > 2$. This is consistent with their definitions: the FQA protocol of Eq. (22) does a better job at securing an accurate description of the microscopic dynamics by means of APT, but it does not necessarily give the smallest deviations from the adiabatic theorem. On the other hand, the FQ2 protocol of Eq. (23) gives up some (but not much) of its ability to attain early (for small $\tau$) adiabaticity in order to allow better following of the EOS. Of course, the IIE protocol is built to give the same final state as an adiabatic evolution, and thus gives $K_{\rm ex} = 0$ for any $\tau$.

Figure 5b clearly shows that, when it comes to the energetic cost of the forward process, FQA beats FQ2 for any $\tau$. Thus, in order to closely follow the EOS, one might have to spend more energy throughout the process. Interestingly, IIE gives also $W_{\rm ex} = 0$ for any $\tau$ and, in fact, this can be inferred from the state diagram given in Fig. 4a. The total excess work of a process for a given protocol is the area between its state variable curve and the EOS curve in a state diagram, and we can see that IIE crosses the EOS exactly one time (at $t = (t_f + t_i)/2$). Thus, any excess energy given to the system in the first half of the process (area above the EOS) is retrieved in the second half (area below the EOS), netting zero excess work. This must be the case for any $\tau$, even if the evolution is far from being adiabatic at all times. To illustrate this, we have included Fig. 6, where the effects just described are naturally exacerbated. All in all, IIE accomplishes "finite-time reversibility" when the whole process is taken into account, re-treading its thermodynamic path when time is reversed and dissipating zero energy.

* asorianialves@gmail.com


[1] G. Rigolin, G. Ortiz, and V. H. Ponce, Phys. Rev. A **78**, 052508 (2008).
[2] D. M. Tong, K. Singh, L. C. Kwek, and C. H. Oh, Phys. Rev. Lett. **95**, 110407 (2005).
[3] D. M. Tong, Phys. Rev. Lett. **104**, 120401 (2010).
[4] P. Pfeuty, Ann. Phys. (N.Y.) **57**, 79 (1970).
[5] J. Dziarmaga, Phys. Rev. Lett. **95**, 245701 (2005).
[6] S. Martínez-Garaot, A. Ruschhaupt, J. Gillet, T. Busch, and J. G. Muga, Phys. Rev. A **92**, 043406 (2015).
[7] H. T. Quan and W. H. Zurek, New J. Phys. **12**, 093025 (2010).
[8] K. Husimi, Prog. Theor. Phys. **9**, 381 (1953).
[9] S. Deffner and E. Lutz, Phys. Rev. E **77**, 021128 (2008).
[10] S. Deffner, O. Abah, and E. Lutz, Chem. Phys. **375**, 200 (2010).
[11] H. R. Lewis Jr. and W. B. Riesenfeld, J. Math. Phys. **10**, 1458 (1969).
[12] X. Chen, A. Ruschhaupt, S. Schmidt, A. del Campo, D. Guéry-Odelin, and J. G. Muga, Phys. Rev. Lett. **104**, 063002 (2010).

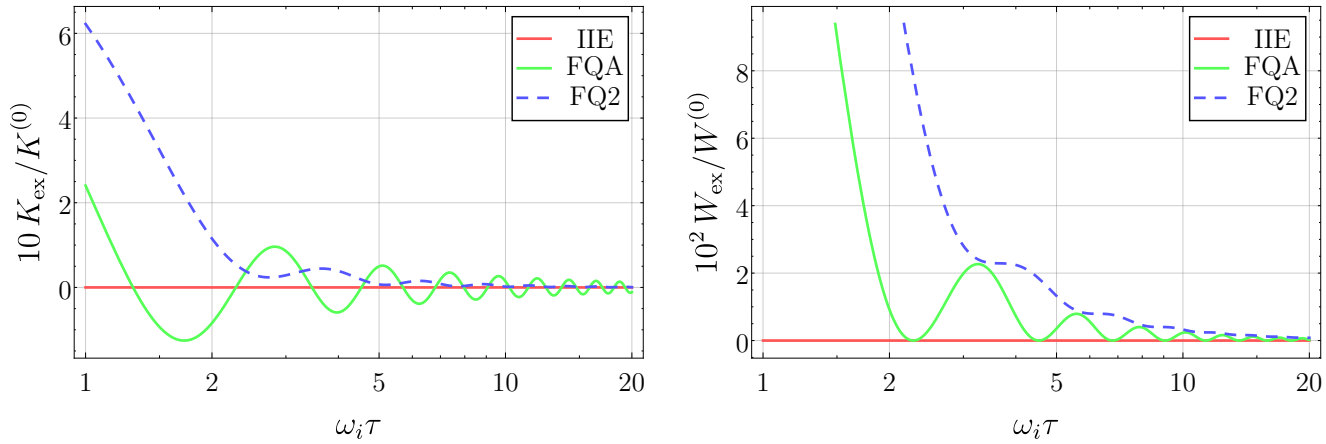


(a) (b)

FIG. 5. (a) Excess state variable vs. $\tau$ for the HO forward process. (b) Excess work vs. $\tau$ for the HO forward process.

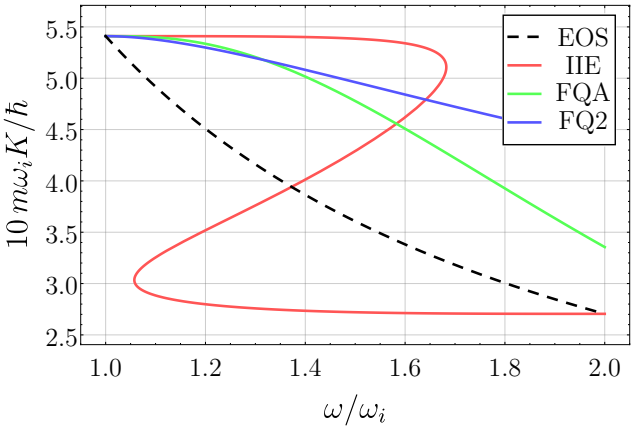


FIG. 6. State diagram for the HO forward process with $\omega_i\tau = 1$, starting from the top left corner.